Hydrol. Earth Syst. Sci. Discuss., 12, 1153–1188, 2015
www.hydrol-earth-syst-sci-discuss.net/12/1153/2015/
doi:10.5194/hessd-12-1153-2015
© Author(s) 2015. CC Attribution 3.0 License.

Hydrology and Earth System Sciences Discussions
Open Access

This discussion paper is/has been under review for the journal Hydrology and Earth System Sciences (HESS). Please refer to the corresponding final paper in HESS if available.

# Role of vegetation and landcover dynamics on the recycling of water in two endorheic watersheds of NW China (Gansu Province)

**M. A. Matin[1] and C. P.-A. Bourque[1,2]**

[1]Faculty of Forestry and Environmental Management, University of New Brunswick, 28 Dineen Drive, P.O. Box 4400, Fredericton, New Brunswick, E3B 5A3, Canada
[2]The School of Soil and Water Conservation, Beijing Forestry University, 35 East Qinghua Road, Haidan District, Beijing, 100083, China

Received: 5 January 2015 – Accepted: 7 January 2015 – Published: 26 January 2015

Correspondence to: C. P.-A. Bourque (cbourque@unb.ca)

Published by Copernicus Publications on behalf of the European Geosciences Union.

## Abstract

In this study, we analysed the role of vegetation in the recycling of water in two endorheic watersheds in northwest China, namely within the Shiyang and Hei River watersheds (Gansu Province), along a gradient of elevation zones and within-zone landcover types. Each watershed was subdivided into four elevation zones representative of (i) oasis plains and foothills, and (ii) low-, (iii) mid-, and (iv) high-mountain elevations. By means of monthly summaries of enhanced vegetation index (EVI), DEM-height values, terrain orientation, and a decision-tree classifier, landcover in the study area (consisting of oases, deserts, and adjoining Qilian Mountains) was classified into 11 unique landcover types. Comparison of monthly vegetation phenology with precipitation and snowmelt dynamics within the same watersheds over a ten-year period (2000–2009) suggested that the onset of the precipitation season in the mountains (in May) was triggered by the greening of vegetation and increased production of water vapour at the base of the mountains. Seasonal evolution of in-mountain precipitation correlated fairy well with the temporal variation in oasis-vegetation coverage and phenology (of crops and grasses) characterised by monthly EVI, giving $r^2$ values of 0.65 and 0.85 for the Shiyang and Hei River watersheds, respectively. Generally, comparisons between same-zone monthly precipitation volumes and EVI provided weaker correlations. Start of the growing season in the oases was shown to coincide with the discharge of meltwater from the low- to mid-elevations of the Qilian Mountains in mid-to-late March. Comparison of water volumes associated with in-mountain production of rainfall and snowmelt with that associated with actual evapotranspiration revealed that about 90 % of the water flowing downslope to the oases was eventually returned to the Qilian Mountains as water vapour generated in the lowlands.





HESSD
12, 1153–1188, 2015

## 1 Introduction

River basins not connected to oceans (endorheic basins; Meybeck, 2003) occupy about 13 % of the total land surface of the earth (Meybeck et al., 2001) and generate about 2.3 % of global runoff (Shiklomanov, 1998). Most of these basins are located in water-limited regions of the world, generally in the middle of continents far from oceanic sources of moisture or blocked by mountain ranges (Meybeck et al., 2001). In endorheic basins, located in arid mountainous regions, water is mostly generated in the mountains, which eventually flows downslope to terminate in deserts (X. Li et al., 2013). These basins are extremely sensitive to landcover and climate variability (Meybeck, 2003). Therefore, understanding the water cycle in these areas is extremely important for the long term sustainability (Pilgrim et al., 1988) of desert oases in northwest (NW) China.

The influence of landuse practices and landcover (LULC) on local and regional climate has been widely demonstrated in the scientific literature (Bourque and Hassan, 2009; Helldén, 2008; Pielke and Avissar, 1990). Changes in LULC lead to changes in surface albedo, roughness length, leaf area index (LAI), and rooting depth, and changes in the energy and water balance of the land surface (Beltran-Przekurat et al., 2012; Pielke et al., 2007b). For example, reduction in surface albedo can cause the net radiation at the surface to increase by reducing the amount of shortwave radiation reflected by the surface, leading to a greater amount of surface energy available for sensible, latent, and ground heat (Cotton and Pielke, 2007). Changes in surface properties can also influence climate by modifying the evaporative fraction of the surface and partitioning of net radiation into sensible and latent heat (Greene et al., 1999; Pielke, 2001; Pielke et al., 2007a; Raddatz, 2007). Variations in precipitation and latent heat can lead to alterations in infiltration and surface and shallow sub-surface flow (Fernandez-Illescas and Rodriguez-Iturbe, 2004; Porporato et al., 2002; Ridolfi et al., 2006; Wilcox et al., 2003, 1997). The role of vegetation on soil moisture and runoff is also fairly well described in the scientific literature (e.g. Fernandez-Illescas





HESSD
12, 1153–1188, 2015



cc BY

and Rodriguez-Iturbe, 2004; Porporato et al., 2002; Ridolfi et al., 2006; Wilcox et al., 2003, 1997).

Vegetation itself is influenced by the variability in hydro-climatic conditions. For example, variation in precipitation, snowmelt, and surface runoff can have a profound effect on the availability of soil moisture, which, in turn, can affect the growth of vegetation and its distribution in water-limited environments (Fernandez-Illescas and Rodriguez-Iturbe, 2004). Understanding the mutual interactions between vegetation and hydro-climatic variables is fundamental to modelling eco-hydrometeorological processes in excessively dry environments.

By simulating regional climate over China, Gao et al. (2003) have shown that landuse changes has decreased precipitation levels in NW China by about 20 %. In a similar analysis, Ming and Xinmin (2002) have shown that deforestation and degradation of agricultural lands could potentially lead to desertification of northern China; afforestation of affected lands could potentially reverse this trend. However, Sen et al. (2004) have demonstrated that once in a desert state, re-greening of the landscape is difficult to achieve through afforestation, as the transplanted vegetation is itself influenced by the hydro-climatic conditions existing at the time of planting. By model simulation, Bourque and Hassan (2009) have shown that the reduction of vegetation in oases in NW China, beyond a critical threshold, is irrecoverable because it results in significant loss of atmospheric water vapour returning to the oases as surface and shallow sub-surface flow.

The objective of this paper is to investigate the relative influence of oasis vegetation on water recycling and the generation of in-mountain precipitation in two large endorheic watersheds in NW China over a ten-year period (2000–2009). Spatiotemporal variation in oasis-vegetation coverage and phenology is characterised by a chronological series of monthly MODIS (Moderate Resolution Imaging Spectroradiometer)-based images of enhanced vegetation index (EVI; Huete et al., 2002) and landcover-specific thresholds. Hydrological components central to the analysis, include monthly surfaces of actual evapotranspiration (AET), precipitation, snowmelt, and mountain return flow





HESSD
12, 1153–1188, 2015

(i) developed in part from remote sensing (RS)-products and modelling procedures, and (ii) validated against field data collected at climate and hydrometric stations (Fig. 1 in Sirikul, 2006) described in Matin and Bourque (2013a, b, 2015).

## 2 Study area

The study area consists of the Shiyang and Hei River watersheds in westcentral Gansu Province, NW China (Fig. 1). The Shiyang River watershed is an endorheic river basin (F. Li et al., 2013) located in the eastern Hexi Corridor. The Shiyang River originates from the Qilian Mountains and flows about 300 km northeastward (Gao et al., 2006) before terminating in the Minqin-lake district (Li et al., 2007). The total watershed area is roughly 49 500 km$^2$. Elevation in the Shiyang River watershed varies from 1284–5161 m a.m.s.l. (above mean sea level), with an average elevation of 1871 m a.m.s.l. The Shiyang River system has eight main branches, including the Xida, Donga, Xiying, Jinta, Zamusi, Huangyang, Gulang, and Dajing Rivers (F. Li et al., 2013; Wonderen et al., 2010).

The Hei River also originates from the Qilian Mountains, northwest of the headwaters of the Shiyang River network, and flows northwestward through the oases and terminates in the desert lakes (Akiyama et al., 2007). The Hei River watershed, with a land surface area of approximately 128 000 km$^2$, is the second largest endorheic watershed in NW China (Gu et al., 2008). The Hei River watershed includes the Zhangye sub-watershed, with a total land area of about 31 100 km$^2$. Elevation in the Zhangye sub-watershed varies from 1287–5045 m a.m.s.l., with an average elevation of 2679 m a.m.s.l.

The study area overlaps four distinct ecoregions (Olson et al., 2001). The northern part, noted for its semi-arid to arid conditions, includes portion of the Badain Jaran and Tengger deserts and oases in the southwestern portions of the Alashan Plateau. Liangzhou Oasis, at the south, and Minqin Oasis, at the north, are two important oases in the Shiyang River watershed (Li et al., 2007). Zhangye Oasis is the main oasis in





HESSD
12, 1153–1188, 2015



M. A. Matin and C. P.-A. Bourque



CC BY

the Zhangye sub-watershed. Spring wheat is the main food crop grown in these oases, which is usually supported by irrigation (Zhao et al., 2005). In the deserts, salt-tolerant, xerophytic shrub species, i.e. saxaul (*Haloxylon ammodendron*) and *Reaumuria soongolica* (Carpenter, 2015a) are commonly found. North-facing slopes of the Qilian Mountains (Fig. 1) support alpine meadow at elevations ≤ 3300 m a.m.s.l. and deciduous shrubland at elevations > 3300 m a.m.s.l. Isolated patches of conifer forests (mostly of Qinghai spruce; *Picea crassifolia*) in the Qilian Mountains are classified as a separate ecoregion (Carpenter, 2015b). The natural landscape of the study area comprises of mountains, oases, and deserts, all interacting with one another (Ma and Veroustraete, 2006).

The study area includes five morphologic units, including mountains, foothill country, alluvial fans, plain, and terminal lakes (Gao et al., 2006). Umbric soils are the dominant soil type in the oases of both watersheds, i.e. Umbric Leptosols in the Shiyang River and Umbric Leptosols and Umbric Gleysols in the Hei River watersheds. Soil types in the mountains generally vary as a function of elevation. Dominant soil groups in the Qilian Mountains are Cambisols, Luvisols, Gleysols, and Pedozols (Nachtergaele et al., 2012). The oases are mostly flat with an average slope $< 5^{\circ}$, whereas mountainous regions are highly undulated; roughly 40 % of the region has slopes $> 15^{\circ}$.

Locally-generated precipitation in the oases is normally inadequate (120–170 mm yr$^{-1}$ based on 30 years of data collected from 1976–2005; Matin and Bourque, 2013a) to support agriculture. The key source of water to the oases is the runoff from the Qilian Mountains generated from snowmelt and in-mountain rainfall carried by the Shiyang River and Hei River systems (Jin et al., 2010; Wang et al., 2009). Glacial meltwater on average contributes to about 3.8 and 8.3 % of total runoff in the Shiyang and Hei Rivers, respectively (Wang et al., 2009).

Meltwater in rivers usually flows during late-spring to mid-summer due to the melting of the previous snow-season's snow cover and warming of the mountain glaciers (Ji et al., 2006). A primary source of water to the rivers during the summer is orographic precipitation (Roe, 2005) formed in the Qilian Mountains (Zhu et al., 2004).





HESSD
12, 1153–1188, 2015



M. A. Matin and C. P.-A. Bourque



CC BY

Long term average data (1950–2000) show that precipitation and potential evaporation (PET) in the deserts are approximately 80–150 mm $yr^{-1}$ and 2300–2600 mm $yr^{-1}$ (based on an application of the Penman–Monteith equation, Monteith, 1965; Penman, 1948). Precipitation increases in the mountains from 300–600 mm $yr^{-1}$, while PET decreases to about 700 mm $yr^{-1}$ (Akiyama et al., 2007; Chen et al., 2005; Gates et al., 2008; Huo et al., 2008; Kang et al., 2009; Ma et al., 2013; Tong et al., 2007; Wang and Cheng, 1999; Wang and Zhao, 2011; Zang et al., 2012). Most of the precipitation occurs during June–August. About 94 % of water delivered from the mountains to lowland oases is through surface runoff. Average annual runoff in the Shiyang River is about $15.8 \times 10^8$ $m^3$ $yr^{-1}$, whereas in the Hei River it is about $37.7 \times 10^8$ $m^3$ $yr^{-1}$ (Kang et al., 2009).

Vegetation in the oases and lower mountains plays an important role in maintaining the hydrological cycle by assisting AET. Interruption of the region's vegetative cover could potentially lead to a disruption in the eco-hydrological balance in the recycling of water (Bourque and Hassan, 2009) that must be supplemented by the unsustainable extraction of groundwater (Currell et al., 2012; Qin et al., 2012). Dependency of the local water cycle on lowland oasis vegetation is supported by many other studies, including those of Huo et al. (2008), Jia et al. (2011), Kang et al. (1999), Li et al. (2008), Ma et al. (2013).

## 3 Methods

Vegetation characteristics generated from monthly RS-based estimates of EVI were compared and analysed with respect to monthly estimates of precipitation, AET, and snowmelt, generated from earlier studies (Matin and Bourque, 2013a, b, 2015). Figure 2 describes the workflow (inputs and their usage) and associated results of this study.





HESSD
12, 1153–1188, 2015



cc BY

## 3.1 Vegetation characteristics

### 3.1.1 Landcover

The MODIS-based annual global landcover map currently available (as of 2012) is produced from seven spectral maps, bi-directional reflectance distribution function (BRDF)-adjusted reflectance, land surface temperature ($T_s$), EVI, and an application of supervised classification using ground data from 1860 field sites (Friedl et al., 2010). Assessments of the product have shown that this map is not entirely realistic for zones of steep transition, particularly in mountainous areas (Liang and Gong, 2010). Improved landcover definition at regional or local scales with supervised classification usually involves much greater amounts of ground data that are normally available for most regions. Recently, decision tree-based classifications have been applied to RS-data and has been shown to produce better results than other classification systems based on maximum likelihood or unsupervised clustering and labelling (Friedl and Brodley, 1997). One benefit of decision tree-based classification is that it is able to use local knowledge of vegetation characteristics together with other pertinent information, such as terrain characteristics, in its evaluation. In the current study, chronological-sequences of MODIS-based EVI and digital terrain information of the study area (e.g. slope orientation, elevation) are used to classify landcover with a decision-tree classifier.

Vegetation distribution in the study area has a unique preferential association with elevation, slope, and slope direction (Jin et al., 2008). For instance, north-facing slopes of the Qilian Mountains support alpine meadow at elevations between 2500 to 3300 m a.m.s.l. At elevations > 3300 m a.m.s.l., deciduous shrubs represent the most dominant vegetation type. Isolated patches of conifer forests in the Qilian Mountains are found at elevations between 2500 m to 3300 m a.m.s.l. (Carpenter, 2015b). Seasonal vegetation density and growth vary as a function of landcover and elevation.

Based on vegetation site preferences, the study area was subdivided into four main elevation zones, defined by elevations: (i) < 2500 (oasis plains and foothills; Zone 1),





HESSD
12, 1153–1188, 2015



M. A. Matin and C. P.-A. Bourque



cc BY

(ii) 2500–3300 (low-mountain elevations; Zone 2), (iii) 3300–3900 (mid-mountain elevations; Zone 3), and (iv) > 3900 m a.m.s.l. (high-mountain elevations; Zone 4). Different landcover types in these elevation zones were then identified based on EVI and slope orientation. Landcover types and their discrimination are summarised in Table 1.

Ten landcover maps were generated for 2000–2009. From these maps, a final landcover composite ($\mathrm{LCOV_{dom}}$ for all image pixels; Fig. 1) was then created based on a pixel-level, landcover-dominance evaluation, i.e.

$$\mathrm{LCOV_{dom}}\Big|_{\text{for all pixels}} = \underset{i=2000-2009}{\mathrm{Majority}}\left(\mathrm{LCOV}_i\right)\Big|_{\text{for all pixels}}, \tag{1}$$

where $\mathrm{LCOV}_i$ and $\mathrm{LCOV_{dom}}$ represent landcover at the pixel-level for individual years (2000 through 2009) and the dominant landcover over the same ten-year time period, respectively.

### 3.1.2 Vegetation phenology

Land surface phenology (LSP) refers to the timing of different life-cycle stages of plants (Martinez and Gilabert, 2009). Seasonal changes in LSP is important to understand the relationship between vegetation growth and the hydrological cycle in watersheds (Martinez and Gilabert, 2009). Study of LSP is also important to understand the causes of vegetation-growth-pattern changes (Fisher and Mustard, 2007; Myneni et al., 1997). Satellite-based analysis of LSP addresses the development patterns in photosynthetic biomass by means of derived vegetation indices (Ahl et al., 2006) in an area that can potentially support many species. Ground-based analysis of LSP, in contrast, focusses on a single tree species at a time.

Typical measures of phenology are (i) onset of greening, (ii) onset of senescence, (iii) peak development, during the growing season, and (iv) length of the growing season (Hudson et al., 2010). Various methods have been adopted to assess phenology from space. Hudson et al. (2010) classified these into four groups, namely (i) threshold-, (ii) derivative-, (iii) smoothing-, and (iv) model-based methods. Among these methods, the threshold-based method is the simplest and most commonly used (Hudson et al., 2010).

With the threshold-based method, a single value of vegetation index (VI) is specified as the threshold. The values of VI are plotted against time of year. The time when the threshold value is passed in the upward direction is identified as the start of the growing period and when the same value is passed in the downward direction, the time is identified as the end of the growing period (Karlsen et al., 2006). Methods of selecting the threshold vary among studies. Some authors use single arbitrary thresholds, e.g. 0.17 (Fischer, 1994), 0.09 (Markon et al., 1995), and 0.099 (Lloyd, 1990), whereas some use threshold specifiers like the long term average (Karlsen et al., 2006) or % peak amplitude of VI (Jonsson and Eklundh, 2002).

In the current analysis, phenological state and regional coverage is specified by monthly MODIS EVI. Different thresholds were identified for each landcover type to determine the onset of greening and senescence in the vegetative cover. Threshold values were generated from spatially-distributed 10 year averages of monthly mean EVI. Zonal averages of mean EVI were calculated for each landcover for each month of the year. These values were plotted against time to generate separate EVI-vs.-time plots for each landcover type. The threshold values were specified at the time when mean EVI had maximum positive curvature when moving in the upward direction. Values generated were 0.09 for crop and sparse grass, 0.17 for coniferous forest and meadow, and 0.12 for other vegetation types.

### 3.2 Onset, cessation, and duration of the precipitation season

Most methods used in establishing the onset and cessation of the precipitation season, usually aim to determine the effective planting date of crops (Adejuwon et al., 1990; Adejuwon and Odekunle, 2006; Benoit, 1977; Ilesanmi, 1972). In these methods, the onset and end of the precipitation season is equated to the onset and end of the growing season (Benoit, 1977; Odekunle et al., 2005). These methods do not help elucidate the relationship between the onset of the growing and precipitation seasons,





HESSD
12, 1153–1188, 2015



CC BY

when the seasons are not entirely synchronised. Cumulative % precipitation (Ilesanmi, 1972) is the most widely used indicator of the onset and cessation of the precipitation season independent of other climatic and vegetation factors (Adejuwon et al., 1990; Adejuwon and Odekunle, 2006; Odekunle, 2006). In this method, daily % precipitation data are processed to generate five-day means. Using these means, cumulative precipitation is plotted against time of year. On these plots, the point of maximum positive curvature is defined as the onset of the precipitation season, whereas the point of maximum negative curvature is defined as the cessation of the season. Point of onset typically happens at the time when cumulated % precipitation is between 7–8 %, while the typical time of cessation is when cumulation reaches about 90 % (Ilesanmi, 1972). In the analysis, we apply Ilesanmi's approach, but to monthly data.

Precipitation data were generated from monthly Tropical Rainfall Measuring Mission (TRMM) data. These data were downscaled and calibrated to produce 250 m resolution precipitation datasets (Matin and Bourque, 2013b). Spatial averages of monthly precipitation were calculated for the same elevation zones as identified earlier, i.e. oases plains and foothills (< 2500 m a.m.s.l.; Zone 1), low-mountain (2500–3300 m a.m.s.l.; Zone 2), mid-mountain (3300–3900 m a.m.s.l.; Zone 3) and high-mountain positions (> 3900 m a.m.s.l.; Zone 4). These values were used to generate cumulative % precipitation curves for each zone as a function of month (Fig. 3).

### 3.3 Evapotranspiration

Using the complementary method of Venturini et al. (2008), monthly AET for the study area was calculated for the period of 2000–2009 (Matin and Bourque, 2013a). To evaluate the influence of vegetation on AET, monthly EVI was compared against the same-month AET. Spatial averages of monthly EVI and AET were calculated for each land-cover type in both watersheds and compared against each other.





HESSD
12, 1153–1188, 2015

### 3.4 Water yield estimation

Zone-specific water yield ($Y$) is calculated as the balance of precipitation, AET, and snowmelt (Matin and Bourque, 2013b), i.e.

$$Y_{i,j}^{k} = P_{i,j}^{k} + \mathrm{SM}_{i,j}^{k} - \mathrm{AET}_{i,j}^{k}, \tag{2}$$

where SM is snowmelt, "$i$" and "$j$" refer to a specific pixel row and column number in rasters, and "$k$" refers to the time of year (i.e. month number). Here, water yield does not take into account the lateral flow of water, but what is generated or lost locally. The yield is positive when the sum of rainfall and snowmelt is greater than AET and negative when AET exceeds the sum of precipitation and snowmelt. Rasters of monthly snowmelt are generated with a snowmelt model that uses precipitation, air temperature, and DEM (based on NASA's Shuttle Radar Topography Mission, SRTM, v. 4 90 m (3 arcsec) digital elevation model) as primary input in the calculation of snowmelt in snow-water equivalence (Matin and Bourque, 2013b).

## 4 Results and discussion

### 4.1 Onset of the growing season

Onset of greening for the different sections of the watersheds for 2000–2009 is illustrated in Fig. 4. In Fig. 5, elevation zone-specific means of EVI are plotted against time of year. From Figs. 4 and 5, it is clear that in the oases, onset of greening occurs mostly in April, except in some parts, where the growing season is slightly advanced (i.e. initiating in March). In the forest and meadow areas of the mountains, the growing season commences in May, and in some parts, in June. Early changes in vegetation development patterns (changes in monthly EVI) seen in the upper mountainous regions of the watersheds (Fig. 4) might occur as a result of localised melting of the snowpack. Vegetation growth reaches its peak in July–August and dies back in all areas of the





HESSD
12, 1153–1188, 2015

study area in November, except in the high-mountain regions of the Hei River watershed, where vegetation senescence occurs in early October. From Fig. 5, it is apparent that the precipitation season starts in May and ends in September with nominal interannual variation in cumulation and timing. Greatest interannual variation is observed to occur in the lowlands (Zone 1) of both watersheds, and the least in the mountains (e.g. Zones 3 and 4). Interannual variation in the lowlands is most likely associated with the convective nature of locally-generated precipitation. Asynchrony in the start of the oasis-vegetation growing and in-mountain precipitation seasons by about one month (the growing season in the oases starting earlier), suggests that oasis-vegetation development and seasonal build-up of AET sufficient to trigger the precipitation season in the Qilian Mountains requires at least one month of active plant growth to ensue. The source of water to support initial vegetation growth in the oases is surface water generated by snowmelt in the lower mountain positions during the March–April period of each year (Fig. 6). Meltwater production in the lower mountainous portions of both watersheds is about the same (i.e. $250 \times 10^6\,m^3$ in the Shiyang vs. $223 \times 10^6\,m^3$ in the Hei River watersheds, respectively), whereas it is greatest in the mid- to high-mountainous portions of the Hei River watershed ($299 \times 10^6\,m^3$ in the Shiyang vs. $1129 \times 10^6\,m^3$ in the Hei River watershed) as a result of differences in their respective effective surface areas at those elevations, i.e. 2979 vs. 10 328 $km^2$ for the Shiyang and Hei River watersheds.

### 4.2 Vegetation influence on AET

Scattergraphs illustrating average regional AET as a function of average EVI over the growing season (April–October) suggest that regional AET has strongest positive correlation with vegetation in the oases with very high $r^2$ values for crops and dense grass (Fig. 7). Correlation with landcover types in the mountains is also positive, but much weaker. Correlations between vegetation and AET reveal that the amount of vegetation in the oases (with respect to crops and dense grass) is an important contributing factor to defining the amount of water vapour released into the atmosphere.





HESSD
12, 1153–1188, 2015



CC BY

### 4.3 Vegetation influences on precipitation

To evaluate the influence of vegetation on precipitation, spatial averages of monthly precipitation for the different elevation zones are compared with oasis monthly EVI (Fig. 8) and AET (Fig. 9). Comparisons are also made between zone-specific precipitation with same-zone EVI and AET. Coefficients of determination for these comparisons are given in Table 2. These comparisons reveal that within-zone vegetation has a weak influence on precipitation generated locally (i.e. in the same zone; Table 2), but precipitation in the mountains has the strongest correlation with vegetation and AET in the oases (Figs. 8 and 9). Correlation becomes strongest in the high mountains. These results tend to support the suggestion that water vapour production by the oases is responsible for the generation of precipitation in the Qilian Mountains.

### 4.4 Zone-specific water yield

Spatial averages of monthly water yield for the different elevation zones were calculated and plotted against time (Fig. 10). In the oases, AET production by crops and grasses exceed locally-generated precipitation. Comparisons between annual cumulative water volumes associated with the sum of rainfall and snowmelt with those of AET for corresponding elevation zones and for the total watershed show that annual water volumes associated with AET exceeds those of rainfall + snowmelt in the oases (i.e. rainfall + snowmelt – AET < 0.0), with the opposite being the case in the mountains (i.e. rainfall + snowmelt – AET > 0.0). Differences in the mountains (rainfall + snowmelt – AET) tend to increase with increased elevation because of corresponding increases in rainfall and snowmelt (to a certain elevation threshold; Matin and Bourque, 2013b) and decreases in AET. Total water volume associated with rainfall and snowmelt collectively is about equal to that of AET at the watershed level, i.e. 90 and 89 % for the Shiyang and Hei River watersheds, respectively (Table 3). This suggests that the bulk of water originating from the mountains (~ 90 %) is eventually returned to the mountains as evaporated water. This water can travel across watershed boundaries, but once de-





HESSD
12, 1153–1188, 2015



cc BY

posited, surface water is mostly confined to the watershed. This result is consistent with a hydrologically-closed system.

## 5 Conclusions

This paper analyses the interdependencies between different components of the hydrological cycle of the Shiyang and Hei River study watersheds. By correlating precipitation, AET, and vegetation within different elevation zones of the watersheds, the analysis reveals that oasis vegetation has an important role in sustaining the water cycle in both watersheds. Oasis vegetation is dependent on surface water flowing to the region from mountain surface and shallow-subsurface sources. Surface runoff is generated from the precipitation falling in the adjoining mountains. Correlation analysis shows that in-mountain-generated precipitation is strongly correlated to the state of oasis vegetation ($r^2 = 0.65$ and 0.85 for the Shiyang and Hei River watershed, respectively) and water vapour generated by AET ($r^2 = 0.57$ and 0.77). Comparisons between the onset of vegetation development and the precipitation season shows that the growing season precedes the precipitation season in the oases by about one month. This suggests that vegetation growth in the oases provides a biotic trigger for the initiation of the precipitation season in the mountains. Onset of vegetation development in the oases is supported by the generation of snowmelt in the mountains in March-April. Analysis of annual total water volume involved at the watershed level seems to indicate that rainfall and snowmelt together, integrated across the entire watersheds, accounts for about 90 % of water transported to the mountains as a result of AET in the oases.

*Author contributions.* The first author Mir Matin, designed the study, processed data and wrote the paper. The Second author Charles Bourque provided guidance for study formulation and edited the manuscript.





HESSD
12, 1153–1188, 2015



CC BY

*Acknowledgements.* This study was jointly funded by: (i) Lanzhou Regional Climate Centre of the Gansu Provincial Meteorological Bureau (GMB), Lanzhou, China (Natural Science Foundation of China, Grant Number 40830957), (ii) the Natural Science and Engineering Research Council of Canada (NSERC) through a Discovery Grant to CPAB; and (iii) the Faculty of Forestry and Environmental Management, University of New Brunswick, New Brunswick, Canada with its financial support of MAM in the form of graduate-student research and teaching assistantships. We would like to acknowledge the US National Aeronautics and Space Administration (NASA) and Geological Survey (USGS) for providing MODIS-data and SRTM v. 4 DEM-data free of charge.

## References

Adejuwon, J. O. and Odekunle, T. O.: Variability and the Severity of the "Little Dry Season" in Southwestern Nigeria, J. Climate, 19, 483–493, doi:10.1175/jcli3642.1, 2006.

Adejuwon, J. O., Balogun, E. E., and Adejuwon, S. A.: On the annual and seasonal patterns of rainfall fluctuations in sub-saharan West Africa, Int. J. Climatol., 10, 839–848, doi:10.1002/joc.3370100806, 1990.

Ahl, D. E., Gower, S. T., Burrows, S. N., Shabanov, N. V., Myneni, R. B., and Knyazikhin, Y.: Monitoring spring canopy phenology of a deciduous broadleaf forest using MODIS, Remote Sens. Environ., 104, 88–95, doi:10.1016/j.rse.2006.05.003, 2006.

Akiyama, T., Sakai, A., Yamazaki, Y., Wang, G., Fujita, K., Nakawo, M., Kubota, J., and Konagaya, Y.: Surfacewater-groundwater interaction in the Heihe River Basin, Northwest China, Bull. Glaciol. Res., 24, 87–94, 2007.

Beltran-Przekurat, A., Pielke, R. A., Eastman, J. L., and Coughenour, M. B.: Modelling the effects of land-use/land-cover changes on the near-surface atmosphere in southern South America, Int. J. Climatol., 32, 1206–1225, doi:10.1002/Joc.2346, 2012.

Benoit, P.: The start of the growing season in Northern Nigeria, Agr. Meteorol., 18, 91–99, doi:10.1016/0002-1571(77)90042-5, 1977.

Bourque, C. P.-A. and Hassan, Q. K.: Vegetation control in the long-term self-stabilization of the Liangzhou Oasis of the upper Shiyang River watershed of westcentral Gansu, Northwest China, Earth Interact., 13, 1–22, doi:10.1175/2009ei286.1, 2009.





HESSD
12, 1153–1188, 2015



CC BY

Carpenter, C.: Deserts and Xeric Shrublands, Asia: China and Mongolia (PA1302), available at: http://www.worldwildlife.org/ecoregions/pa1302 (last access: 19 January 2015), 2015a.
Carpenter, C.: Montane Grasslands and Shrublands, Eastern Asia: Central China (PA1015), available at: http://www.worldwildlife.org/ecoregions/pa1015 (last access: 19 January 2015), 2015b.
Chen, Y., Zhang, D. Q., Sun, Y. B., Liu, X. N., Wang, N. Z., and Savenije, H. H. G.: Water demand management: a case study of the Heihe River Basin in China, Phys. Chem. Earth, 30, 408–419, doi:10.1016/j.pce.2005.06.019, 2005.
Cotton, W. R. and Pielke, R. A.: Human Impacts on Weather and Climate, Cambridge University Press, Cambridge, 2007.
Currell, M. J., Han, D. M., Chen, Z. Y., and Cartwright, I.: Sustainability of groundwater usage in northern China: dependence on palaeowaters and effects on water quality, quantity and ecosystem health, Hydrol. Process., 26, 4050–4066, doi:10.1002/hyp.9208, 2012.
Fernandez-Illescas, C. P. and Rodriguez-Iturbe, I.: The impact of interannual rainfall variability on the spatial and temporal patterns of vegetation in a water-limited ecosystem, Adv. Water Resour., 27, 83–95, doi:10.1016/j.advwatres.2003.05.001, 2004.
Fischer, A.: A model for the seaonal-variations of vegetation indexes in coarse resolution data and its inversion to extract crop parameters, Remote Sens. Environ., 48, 220–230, doi:10.1016/0034-4257(94)90143-0, 1994.
Fisher, J. I. and Mustard, J. F.: Cross-scalar satellite phenology from ground, Landsat, and MODIS data, Remote Sens. Environ., 109, 261–273, doi:10.1016/j.rse.2007.01.004, 2007.
Friedl, M. A. and Brodley, C. E.: Decision tree classification of land cover from remotely sensed data, Remote Sens. Environ., 61, 399–409, 1997.
Friedl, M. A., Sulla-Menashe, D., Tan, B., Schneider, A., Ramankutty, N., Sibley, A., and Huang, X. M.: MODIS Collection 5 global land cover: algorithm refinements and characterization of new datasets, Remote Sens. Environ., 114, 168–182, doi:10.1016/j.rse.2009.08.016, 2010.
Gao, X. J., Luo, Y., Lin, W. T., Zhao, Z. C., and Giorgi, F.: Simulation of effects of land use change on climate in China by a regional climate model, Adv. Atmos. Sci., 20, 583–592, 2003.
Gao, Y., Wang, G., Liu, H., Liu, Z., Lin, W., and Wang, J.: Landform effects the distribution and circular mode on groundwater in Shiyang River basin. Beiging, China, available





cc BY

at: http://en.cgs.gov.cn/Achievement/The34thCongress/Evolutional/18050.htm (last access: 3 July 2013), 2006.

Gates, J. B., Edmunds, W. M., Darling, W. G., Ma, J. Z., Pang, Z. H., and Young, A. A.: Conceptual model of recharge to southeastern Badain Jaran Desert groundwater and lakes from environmental tracers, Appl. Geochem., 23, 3519–3534, doi:10.1016/j.apgeochem.2008.07.019, 2008.

Greene, E. M., Liston, G. E., and Pielke, R. A.: Relationships between landscape, snowcover depletion, and regional weather and climate, Hydrol. Process., 13, 2453–2466, 1999.

Gu, J., Li, X., and Huang, C. L.: Land cover classification in Heihe River Basin with time series MODIS NDVI data, Fifth International Conference on Fuzzy Systems and Knowledge Discovery, Vol. 2, Proceedings, Jinan, Shandong, China, 477–481, doi:10.1109/Fskd.2008.517, 2008.

Helldén, U.: A coupled human-environment model for desertification simulation and impact studies, Global Planet. Change, 64, 158–168, 2008.

Hudson, I. L., Keatley, M. R., Beurs, K., and Henebry, G.: Spatio-temporal statistical methods for modelling land surface phenology, in: Phenological Research, edited by: Hudson, I. L. and Keatley, M. R., Springer, Netherlands, 177–208, 2010.

Huete, A. R., Didan, K., Miura, T., Rodriguez, E. P., Gao, X., and Fereira, L. G.: Overview of the radiometric and biophysical performance of the MODIS vegetation indices, Remote Sens. Environ., 83, 195–213, doi:10.1016/S0034-4257(02)00096-2, 2002.

Huo, Z. L., Feng, S. Y., Kang, S. Z., Li, W. C., and Chen, S. J.: Effect of climate changes and water-related human activities on annual stream flows of the Shiyang river basin in and North-West China, Hydrol. Process., 22, 3155–3167, doi:10.1002/Hyp.6900, 2008.

Ilesanmi, O. O.: Empirical formulation of onset, advance, and retreat of rainfall in Nigeria, J. Trop. Geogr., 34, 17–24, 1972.

Ji, X. B., Kang, E. S., Chen, R. S., Zhao, W. Z., Zhang, Z. H., and Jin, B. W.: The impact of the development of water resources on environment in arid inland river basins of Hexi region, Northwestern China, Environ. Geol., 50, 793–801, doi:10.1007/s00254-006-0251-z, 2006.

Jia, L., Shang, H., Hu, G., and Menenti, M.: Phenological response of vegetation to upstream river flow in the Heihe Rive basin by time series analysis of MODIS data, Hydrol. Earth Syst. Sci., 15, 1047–1064, doi:10.5194/hess-15-1047-2011, 2011.

Jin, X. M., Zhang, Y.-K., Schaepman, M. E., Clevers, J. G. P. W., and Su, Z.: Impact of elevation and aspect on the spatial distribution of vegetation in the qilian mountain area with





HESSD
12, 1153–1188, 2015

Hydrology in endorheic watersheds

M. A. Matin and C. P.-A. Bourque



CC BY

remote sensing data, The International Archives of the Photogrammetry, Remote Sensing and Spatial Information Sciences, XXXVII, Part B7, Beijing, 2008.
Jin, X. M., Schaepman, M., Clevers, J., Su, Z. B., and Hu, G. C.: Correlation between annual runoff in the Heihe River to the vegetation cover in the Ejina Oasis (China), Arid Land Res. Manage., 24, 31–41, doi:10.1080/15324980903439297, 2010.
Jonsson, P. and Eklundh, L.: Seasonality extraction by function fitting to time-series of satellite sensor data, IEEE T. Geosci. Remote, 40, 1824–1832, doi:10.1109/Tgrs.2002.802519, 2002.
Kang, E. S., Cheng, G. D., Lan, Y. C., and Jin, H. J.: A model for simulating the response of runoff from the mountainous watersheds of inland river basins in the arid area of northwest China to climatic changes, Sci. China Ser. D, 42, 52–63, doi:10.1007/Bf02878853, 1999.
Kang, S. Z., Su, X. L., Tong, L., Shi, P. Z., Yang, X. Y., Abe, Y. K., Du, T. S., Shen, Q. L., and Zhang, J. H.: The impacts of human activities on the water-land environment of the Shiyang River basin, an arid region in northwest China, Hydrolog. Sci. J., 49, 413–427, doi:10.1623/hysj.49.3.413.54347, 2009.
Karlsen, S. R., Elvebakk, A., Hogda, K. A., and Johansen, B.: Satellite-based mapping of the growing season and bioclimatic zones in Fennoscandia, Global Ecol. Biogeogr., 15, 416–430, doi:10.1111/j.1466-822x.2006.00234.x, 2006.
Li, F., Zhu, G., and Guo, C.: Shiyang River ecosystem problems and countermeasures, Agr. Science, 4, 72–78, doi:10.4236/as.2013.42012, 2013.
Li, X., Cheng, G., Liu, S., Xiao, Q., Ma, M., Jin, R., Che, T., Liu, Q., Wang, W., Qi, Y., Wen, J., Li, H., Zhu, G., Guo, J., Ran, Y., Wang, S., Zhu, Z., Zhou, J., Hu, X., and Xu, Z.: Heihe watershed allied telemetry experimental research (HiWATER): scientific objectives and experimental design, B. Am. Meteorol. Soc., 94, 1145–1160, doi:10.1175/BAMS-D-12-00154.1, 2013.
Li, X. Y., Xiao, D. N., He, X. Y., Chen, W., and Song, D. M.: Factors associated with farmland area changes in arid regions: a case study of the Shiyang River Basin, Northwestern China, Front. Ecol. Environ., 5, 139–144, doi:10.1890/1540-9295(2007)5[139:Fawfac]2.0.Co;2, 2007.
Li, Z. L., Xu, Z. X., Li, J. Y., and Li, Z. J.: Shift trend and step changes for runoff time series in the Shiyang River Basin, Northwest China, Hydrol. Process., 22, 4639–4646, doi:10.1002/Hyp.7127, 2008.
Liang, L. and Gong, P.: An assessment of MODIS collection 5 global land cover product for Biol. Conserv. studies, 18th International Conference on Geoinformatics 2010, Beijing, 2010.







CC BY

Lloyd, D.: A phenological classification of terrestrial vegetation cover using shortwave vegetation index imagery, Int. J. Remote Sens., 11, 2269–2279, 1990.
Ma, J. Z., Chen, L. H., He, J. H., Zhang, Y. R., Li, X. H., and Edmunds, W. M.: Trends and periodicities in observed temperature, precipitation and runoff in a desert catchment: case study for the Shiyang River Basin in Northwestern China, Water Environ. J., 27, 86–98, doi:10.1111/j.1747-6593.2012.00329.x, 2013.
Ma, M. G. and Veroustraete, F.: Interannual variability of vegetation cover in the Chinese Heihe River Basin and its relation to meterological parameters, Int. J. Remote Sens., 27, 5127–5127, doi:10.1080/01431160601103475, 2006.
Markon, C. J., Fleming, M. D., and Binnian, E. F.: Characteristics of vegetation phenology over the Alaskan landscape using time-series data, Polar Rec., 31, 179–190, 1995.
Martinez, B. and Gilabert, M. A.: Vegetation dynamics from NDVI time series analysis using the wavelet transform, Remote Sens. Environ., 113, 1823–1842, doi:10.1016/j.rse.2009.04.016, 2009.
Matin, M. A. and Bourque, C. P. A.: Assessing spatiotemporal variation in actual evapotranspiration for semi-arid watersheds in northwest China: evaluation of two complementary-based methods, J. Hydrol., 486, 455–465, doi:10.1016/j.jhydrol.2013.02.014, 2013a.
Matin, M. A. and Bourque, C. P. A.: Intra- and inter-annual variations in snow-water storage in data sparse desert-mountain regions assessed from remote sensing, Remote Sens. Environ., 139, 18–34, doi:10.1016/j.rse.2013.07.033, 2013b.
Matin, M. A. and Bourque, C. P. A.: Mountain-river runoff components and their role in the seasonal development of desert-oases in northwest China, J. Arid Environ., submitted, 2015.
Meybeck, M.: Global analysis of river systems: from Earth system controls to anthropocene syndromes, Philos. T. Roy. Soc. B, 358, 1935–1955, doi:10.1098/rstb.2003.1379, 2003.
Meybeck, M., Green, P., and Vorosmarty, C.: A new typology for mountains and other relief classes: an application to global continental water resources and population distribution, Mt. Res. Dev., 21, 34–45, doi:10.1659/0276-4741(2001)021[0034:Antfma]2.0.Co;2, 2001.
Ming, Z. and Xinmin, Z.: A theoretical analysis on the local climate change induced by the change of landuse, Adv. Atmos. Sci., 19, 45–63, doi:10.1007/s00376-002-0033-9, 2002.
Monteith, J. L.: Evaporation and environment, Sym. Soc. Exp. Biol., 19, 205–234, 1965.
Myneni, R. B., Keeling, C. D., Tucker, C. J., Asrar, G., and Nemani, R. R.: Increased plant growth in the northern high latitudes from 1981 to 1991, Nature, 386, 698–702, doi:10.1038/386698a0, 1997.





HESSD
12, 1153–1188, 2015

Hydrology in endorheic watersheds

M. A. Matin and C. P.-A. Bourque



CC BY

Nachtergaele, F., Velthuizen, H. V., Verelst, L., Wberg, D., Batjes, N., Dijkshoorm, K., Engelen, V. V., Fischer, G., Jones, A., Montanarella, L., Petri, M., Prieler, S., Teixeira, E., and Shi, X.:. Harmonized world soil database (version 1.2). Food and Agriculture Organization of the United Nations (FAO), International Institute for Applied Systems Analysis (IIASA), ISRIC – World Soil Information, Institute of Soil Science – Chinese Academy of Sciences (IISCAS), Joint Research Centre of the European Commission (JRC), Laxenburg, Austria, 2012.

Odekunle, T. O.: Determining rainy season onset and retreat over Nigeria from precipitation amount and number of rainy days, Theor. Appl. Climatol., 83, 193–201, doi:10.1007/s00704-005-0166-8, 2006.

Odekunle, T. O., Balogun, E. E., and Ogunkoya, O. O.: On the prediction of rainfall onset and retreat dates in Nigeria, Theor. Appl. Climatol., 81, 101–112, doi:10.1007/s00704-004-0108-x, 2005.

Olson, D. M., Dinerstein, E., Wikramanayake, E. D., Burgess, N. D., Powell, G. V. N., Underwood, E. C., D'Amico, J. A., Itoua, I., Strand, H. E., Morrison, J. C., Loucks, C. J., Allnutt, T. F., Ricketts, T. H., Kura, Y., Lamoreux, J. F., Wettengel, W. W., Hedao, P., and Kassem, K. R.: Terrestrial ecoregions of the world: a new map of life on Earth, Bioscience, 51, 933–938, doi:10.1641/0006-3568(2001)051[0933:teotwa]2.0.co;2, 2001.

Penman, H. L.: Natural evaporation from open water, bare soil and grass, P. Roy. Soc. Lond. A, 193, 120–145, 1948.

Pielke, R. A.: Influence of the spatial distribution of vegetation and soils on the prediction of cumulus convective rainfall, Rev. Geophys., 39, 151–177, 2001.

Pielke, R. A. and Avissar, R.: Influence of landscape structure on local and regional climate, Landscape Ecol., 4, 133–155, doi:10.1007/bf00132857, 1990.

Pielke, R. A., Adegoke, J., Beltran-Przekurat, A., Hiemstra, C. A., Lin, J., Nair, U. S., Niyogi, D., and Nobis, T. E.: An overview of regional land-use and land-cover impacts on rainfall, Tellus B, 59, 587–601, doi:10.1111/j.1600-0889.2007.00251.x, 2007a.

Pielke, R. A., Adegoke, J. O., Chase, T. N., Marshall, C. H., Matsui, T., and Niyogi, D.: A new paradigm for assessing the role of agriculture in the climate system and in climate change, Agr. Forest Meteorol., 142, 234–254, doi:10.1016/j.agrformet.2006.06.012, 2007b.

Pilgrim, D. H., Chapman, T. G., and Doran, D. G.: Problems of rainfall–runoff modeling in arid and semiarid regions, Hydrolog. Sci. J., 33, 379–400, doi:10.1080/02626668809491261, 1988.





HESSD
12, 1153–1188, 2015

Porporato, A., D'Odorico, P., Laio, F., Ridolfi, L., and Rodriguez-Iturbe, I.: Ecohydrology of water-controlled ecosystems, Adv. Water Resour., 25, 1335–1348, doi:10.1016/S0309-1708(02)00058-1, 2002.

Qin, D. J., Zhao, Z. F., Han, L. F., Qian, Y. P., Ou, L., Wu, Z. Q., and Wang, M. C.: Determination of groundwater recharge regime and flowpath in the Lower Heihe River basin in an arid area of Northwest China by using environmental tracers: implications for vegetation degradation in the Ejina Oasis, Appl. Geochem., 27, 1133–1145, doi:10.1016/j.apgeochem.2012.02.031, 2012.

Raddatz, R. L.: Evidence for the influence of agriculture on weather and climate through the transformation and management of vegetation: illustrated by examples from the Canadian Prairies, Agr. Forest Meteorol., 142, 186–202, 2007.

Ridolfi, L., D'Odorico, P., and Laio, F.: Effect of vegetation-water table feedbacks on the stability and resilience of plant ecosystems, Water Resour. Res., 42, W01201, doi:10.1029/2005wr004444, 2006.

Roe, G. H.: Orographic precipitation, Annu. Rev. Earth Pl. Sc., 33, 645–671, 2005.

Sen, O. L., Wang, B., and Wang, Y. Q.: Impacts of re-greening the desertified lands in northwestern China: implications from a regional climate model experiment, J. Meteorol. Soc. Jpn., 82, 1679–1693, doi:10.2151/Jmsj.82.1679, 2004.

Shiklomanov, I. A.: World water resources: a new appraisal and assessment for the 21st Century, UNESCO, available at: http://www.ce.utexas.edu/prof/mckinney/ce385d/Papers/Shiklomanov.pdf (last accesse: 10 July 2013), 1998.

Sirikul, N.: Comparisons of Modis Vegetation Index Products With Biophysical and Flux Tower Measurements, PhD Thesis, The University of Arizona, 198 pp., 2006.

Tong, L., Kang, S. Z., and Zhang, L.: Temporal and spatial variations of evapotranspiration for spring wheat in the Shiyang River Basin in Northwest China, Agr. Water Manage., 87, 241–250, doi:10.1016/j.agwat.2006.07.013, 2007.

Venturini, V., Islam, S., and Rodriguez, L.: Estimation of evaporative fraction and evapotranspiration from MODIS products using a complementary based model, Remote Sens. Environ., 112, 132–141, doi:10.1016/j.rse.2007.04.014, 2008.

Wang, G. X. and Cheng, G. D.: Water resource development and its influence on the environment in arid areas of China – the case of the Hei River basin, J. Arid Environ., 43, 121–131, 1999.





HESSD

12, 1153–1188, 2015

Hydrology in endorheic watersheds

M. A. Matin and C. P.-A. Bourque



cc BY

Wang, J. S., Feng, J. Y., Yang, L. F., Guo, J. Y., and Pu, Z. X.: Runoff-denoted drought index and its relationship to the yields of spring wheat in the arid area of Hexi Corridor, Northwest China, Agr. Water Manage., 96, 666–676, doi:10.1016/j.agwat.2008.10.008, 2009.

Wang, X. and Zhao, C.: Analysis of temporal trends in potential evapotranspiration over Heihe River basin, Presented in 2011 International Symposium on Water Resource and Environmental Protection (ISWREP), 20–22 May 2011, Xi'an, doi:10.1109/iswrep.2011.5893130, 2011.

Wilcox, B. P., Newman, B. D., Brandes, D., Davenport, D. W., and Reid, K.: Runoff from a semiarid ponderosa pine hillslope in New Mexico, Water Resour. Res., 33, 2301–2314, doi:10.1029/97wr01691, 1997.

Wilcox, B. P., Breshears, D. D., and Allen, C. D.: Ecohydrology of a resource-conserving-semiarid woodland: effects of scale and disturbance, Ecol. Monogr., 73, 223–239, doi:10.1890/0012-9615(2003)073[0223:eoarsw]2.0.co;2, 2003.

Wonderen, J. V., Moore, D., Wardlaw, R., Zhongjing, W., Litang, H., and Qingling, S.: Water resources and modelling in the Shiyang River Basin, presented in BHS Third International Symposium, Managing Consequences of a Changing Global Environment, Newcastle, 2010.

Zang, C. F., Liu, J., van der Velde, M., and Kraxner, F.: Assessment of spatial and temporal patterns of green and blue water flows under natural conditions in inland river basins in Northwest China, Hydrol. Earth Syst. Sci., 16, 2859–2870, doi:10.5194/hess-16-2859-2012, 2012.

Zhao, C., Nan, Z., and Cheng, G.: Methods for estimating irrigation needs of spring wheat in the middle Heihe Basin, China, Agr. Water Manage., 75, 54–70, doi:10.1016/j.agwat.2004.12.003, 2005.

Zhu, Y. H., Wu, Y. Q., and Drake, S.: A survey: obstacles and strategies for the development of ground-water resources in arid inland river basins of Western China, J. Arid Environ., 59, 351–367, doi:10.1016/j.jaridenv.2003.12.006, 2004.





HESSD
12, 1153–1188, 2015



cc BY

**Table 1.** Landcover type definition as a function of elevation zone, EVI, and slope orientation.

| Elevation zone* | Landcover | Discrimination thresholds |
|---|---|---|
| Zone 1 | Desert | Maximum growing-season EVI < 0.113 |
| | Crop | Maximum growing-season EVI > 0.27 and minimum growing-season EVI < 0.113 |
| | Dense grass | Maximum growing-season EVI > 0.27, and minimum growing season EVI > 0.113 |
| | Sparse grass and/or shrub | Maximum growing-season EVI between 0.113–0.27 and mean growing season EVI > 0.113 |
| | Bare Soil | Maximum growing-season EVI between 0.113–0.27 and mean growing season EVI < 0.113 |
| Zone 2 | Alpine meadow | Maximum growing-season EVI > 0.27 and on north-facing slopes |
| | Coniferous forest | Maximum growing-season EVI > 0.27, but not on north-facing slopes |
| | Sparse grass and/or shrub | Maximum growing season EVI between 0.113–0.27 |
| | Bare land | Maximum growing-season EVI < 0.113 |
| Zone 3 | Deciduous shrub | Maximum growing-season EVI > 0.27 |
| | Bare land | Maximum growing-season EVI < 0.27 |
| Zone 4 | Sparse shrub | Maximum growing-season EVI > 0.113 |
| | Snow and/or ice | Maximum growing-season EVI < 0.113 |

* Zones are classified according to elevation bands: < 2500 m (Zone 1); 2500–3300 m (Zone 2); 3300–3900 m (Zone 3); and > 3900 m a.m.s.l. (Zone 4).





HESSD
12, 1153–1188, 2015



CC BY

**Table 2.** Coefficients of determination ($r^2$) for comparisons between zone-specific precipitation with corresponding same-month EVI and AET for the Shiyang and Hei River watersheds, respectively.

| Variable | Zone * | | | |
|---|---|---|---|---|
| | 1 | 2 | 3 | 4 |
| Precipitation = $f$(EVI) | | | | |
| Shiyang River | 0.44 | 0.61 | 0.52 | 0.45 |
| Hei River | 0.51 | 0.62 | 0.69 | 0.75 |
| Precipitation = $f$(AET) | | | | |
| Shiyang River | 0.41 | 0.34 | 0.20 | 0.18 |
| Hei River | 0.39 | 0.34 | 0.43 | 0.47 |

* Zones are classified according to elevation bands: < 2500 m (Zone 1); 2500–3300 m (Zone 2); 3300–3900 m (Zone 3); and > 3900 m (Zone 4).





HESSD
12, 1153–1188, 2015

Hydrology in endorheic watersheds

M. A. Matin and C. P.-A. Bourque

**Table 3.** AET as a percentage of the sum of precipitation ($P$) and snowmelt (SM) for corresponding elevation zones in the Shiyang River and Hei River watersheds, respectively.

| Zone* | AET as a % ($P$ + SM) | |
|---|---|---|
| | Shiyang River Watershed | Hei River Watershed |
| 1 | 136 | 210 |
| 2 | 88 | 100 |
| 3 | 58 | 81 |
| 4 | 35 | 62 |
| Entire Mountain Area | 72 | 81 |
| Entire Watersheds | 90 | 89 |

* Zones are classified according to elevation bands, i.e. < 2500 m (Zone 1); 2500–3300 m (Zone 2); 3300–3900 m (Zone 3); and > 3900 m (Zone 4).





HESSD
12, 1153–1188, 2015



CC BY

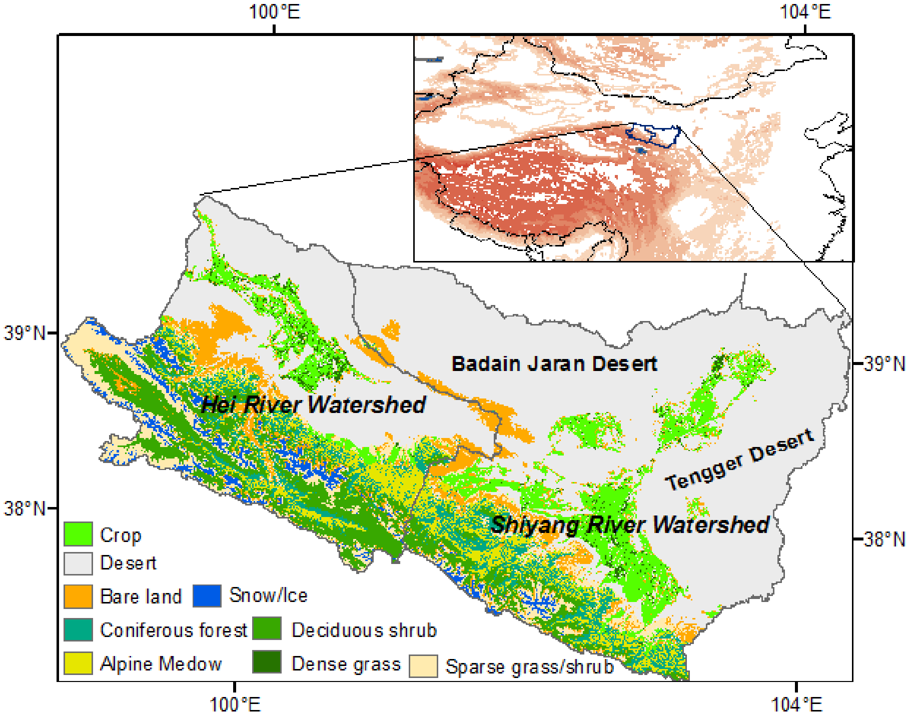


**Figure 1.** The Shiyang and Hei River watersheds with distribution of dominant landcover classes. The inset shows the location of the study area along the northeastern flank of the Qinghai-Tibetan Plateau. Redish-brown colours identify mountain ranges and plateau.





HESSD
12, 1153–1188, 2015



CC BY

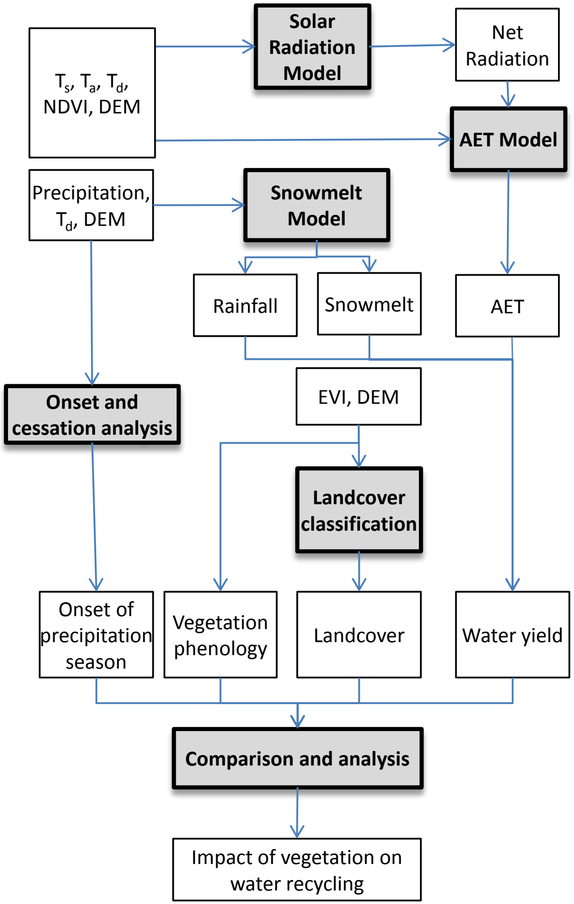


**Figure 2.** Workflow diagram showing input, process, and output in the calculation of the various components of the regional water cycle.





CC BY

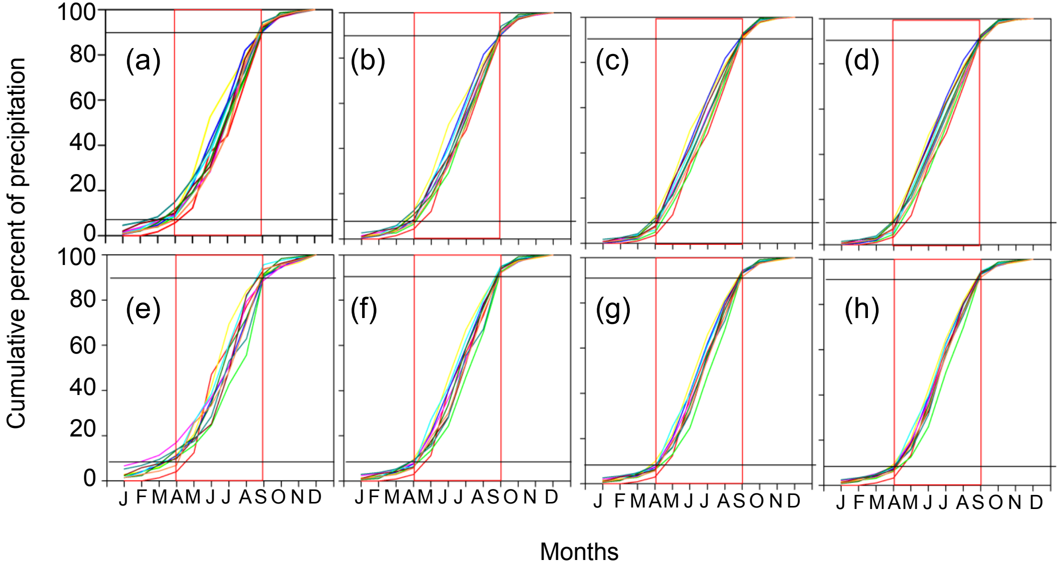


**Figure 3.** Precipitation season onset and cessation in the Shiyang **(a–d)** and Hei River watersheds **(e–h)**, respectively. Cumulative plots for different years are represented in different colours. Plots (**a–d**; upper graphs) and (**e–h**; lower graphs) represent the phenological states in the two watersheds for the **(a, e)** oasis plains and foothills (Zone 1), **(b, f)** low-mountain (Zone 2), **(c, g)** mid-mountain (Zone 3), and **(d, h)** high-mountain portions of the watersheds (Zone 4). The red vertical lines demarcate the onset (first line) and cessation of the precipitation season (second line). The letters along the *x* axis coincide with month, January (J) through to December (D).

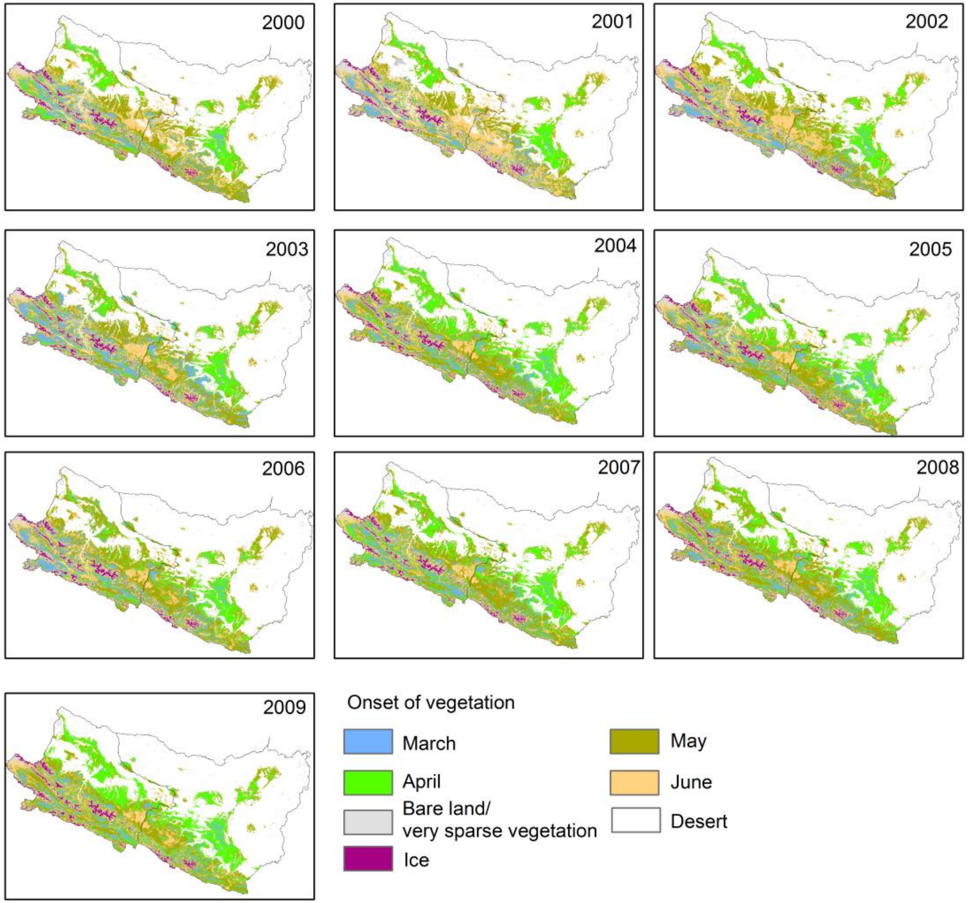


**Figure 4.** Spatial variation in the onset of greening for 2000–2009.



HESSD
12, 1153–1188, 2015

Hydrology in endorheic watersheds

M. A. Matin and C. P.-A. Bourque

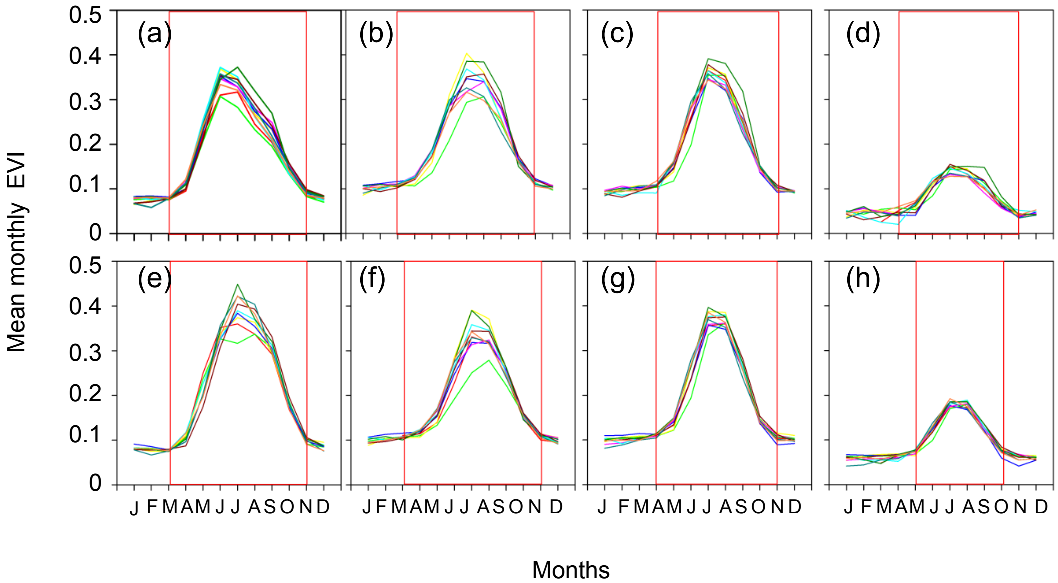


**Figure 5.** Onset, peak, and decline of vegetation growth in the Shiyang **(a–d)** and Hei River watersheds **(e–h)**. Plots (**a–d**; upper graphs) and (**e–h**; lower graphs) represent the phenological conditions in the two watersheds for the **(a, e)** oasis plains and foothills (Zone 1), **(b, f)** low-mountain (Zone 2), **(c, g)** mid-mountain (Zone 3), and **(d, h)** high-mountain portions of the watersheds (Zone 4). The red vertical lines demarcate the onset of greening (first line) and plant senescence (second line). The letters along the *x* axis coincide with month; January (J) through to December (D).





HESSD
12, 1153–1188, 2015

Hydrology in endorheic watersheds

M. A. Matin and C. P.-A. Bourque



CC BY

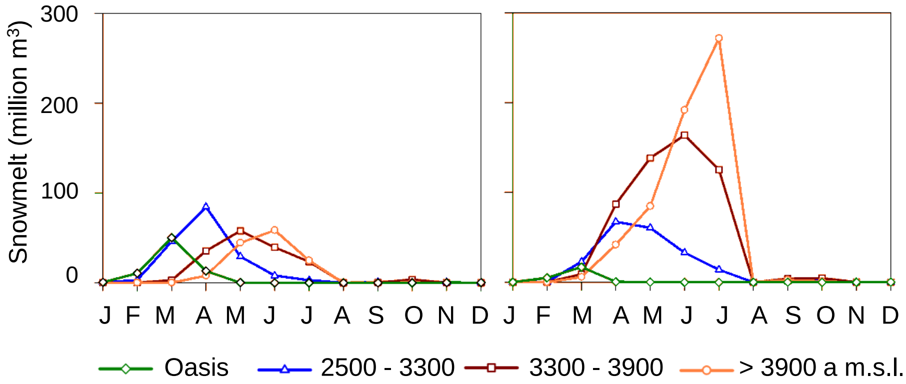


**Figure 6.** Ten-year mean monthly snowmelt generated within the different elevation zones (see legend for colour-elevation zone associations). The first plot applies to the Shiyang River watershed and the second to the Hei River watershed.





HESSD
12, 1153–1188, 2015

Hydrology in endorheic watersheds

M. A. Matin and C. P.-A. Bourque

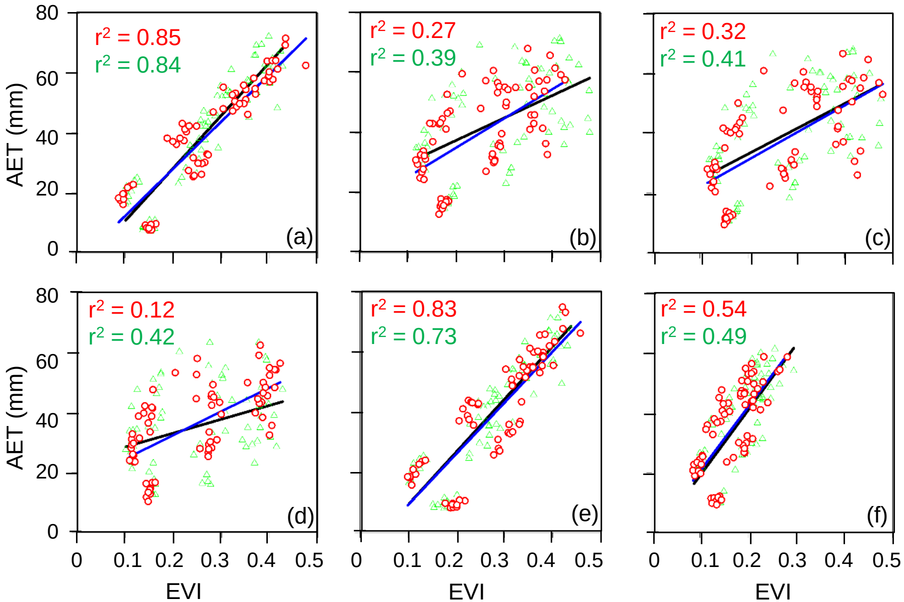


**Figure 7.** Scattergraphs of watershed-level AET as a function of same-month EVI for different vegetation-cover types; red symbols and black solid lines apply to the Shiyang River watershed (first $r^2$ in each plot) and green symbols and blue solid lines to the Hei River watershed (second $r^2$). Landcover types are **(a)** crops, **(b)** coniferous forest, **(c)** alpine meadow, **(d)** deciduous shrubs, **(e)** dense grass in oases, and **(f)** sparse grass and shrubs.

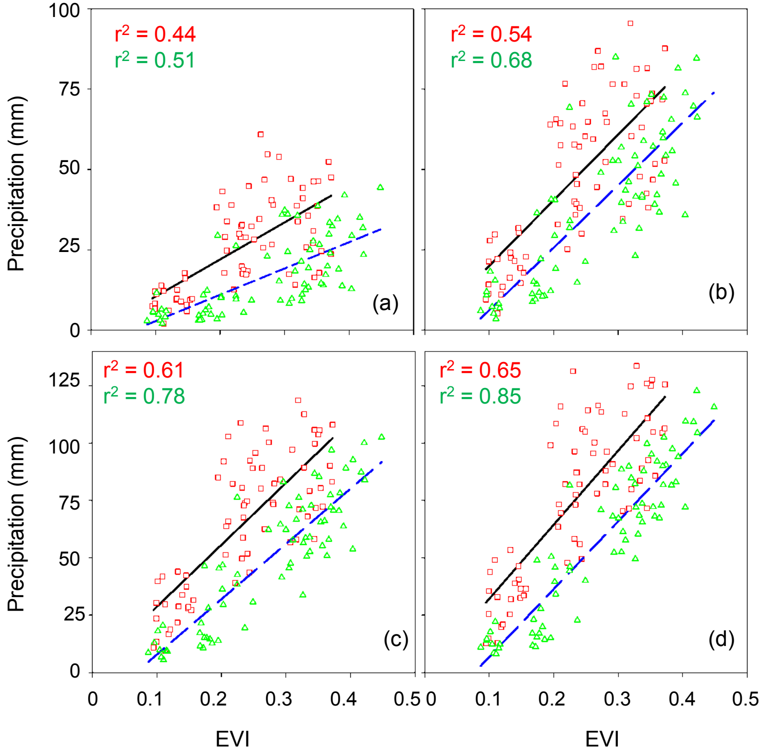


**Figure 8.** Scattergraphs of average precipitation in the different zones as a function of same-month average EVI in the oases; red symbols and black solid lines apply to the Shiyang River watershed (first $r^2$ in each plot) and green symbols and blue dashed lines to the Hei River watershed (second $r^2$). Plots **(a)**–**(d)** coincide with the different elevation zones: **(a)** oasis plains and foothills (Zone 1), and **(b)** low-mountain (Zone 2), **(c)** mid-mountain (Zone 3), and **(d)** high-mountain portion of the watersheds (Zone 4).





HESSD
12, 1153–1188, 2015

Hydrology in endorheic watersheds

M. A. Matin and C. P.-A. Bourque

Title Page
Abstract
Introduction
Conclusions
References
Tables
Figures
◂◂
▸▸
◂
▸
Back
Close
Full Screen / Esc
Printer-friendly Version
Interactive Discussion

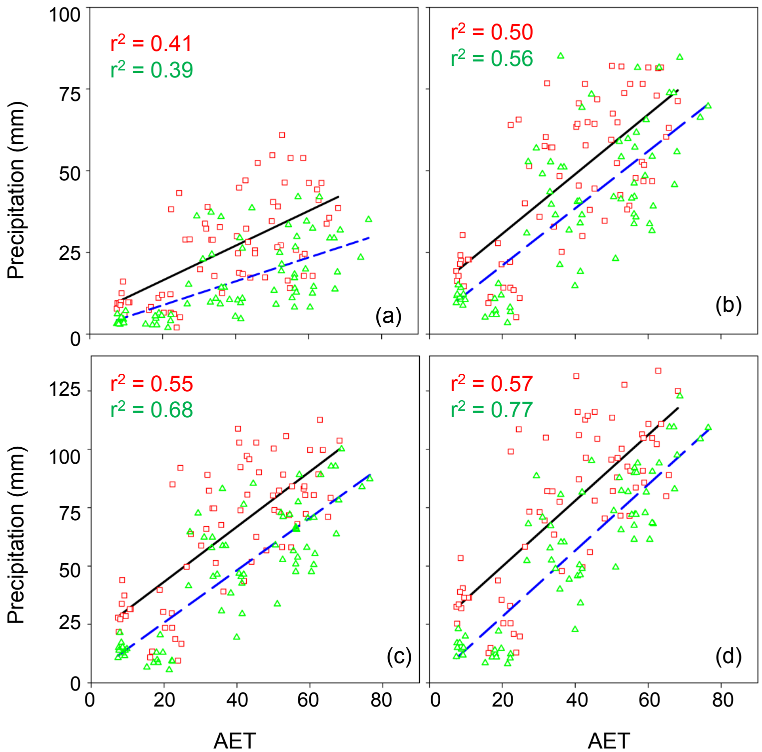


**Figure 9.** Scattergraphs of average precipitation within elevation zones as a function of same-month average AET in the oases; red symbols and black solid lines apply to the Shiyang River watershed (first $r^2$ in each plot) and green symbols and blue dashed lines to the Hei River watershed (second $r^2$). Plots **(a)**–**(d)** coincide with the different elevation zones: **(a)** oasis plains and foothills (Zone 1), and **(b)** low-mountain (Zone 2), **(c)** mid-mountain (Zone 3), and **(d)** high-mountain portions of the watersheds (Zone 4).





HESSD
12, 1153–1188, 2015

Hydrology in endorheic watersheds

M. A. Matin and C. P.-A. Bourque

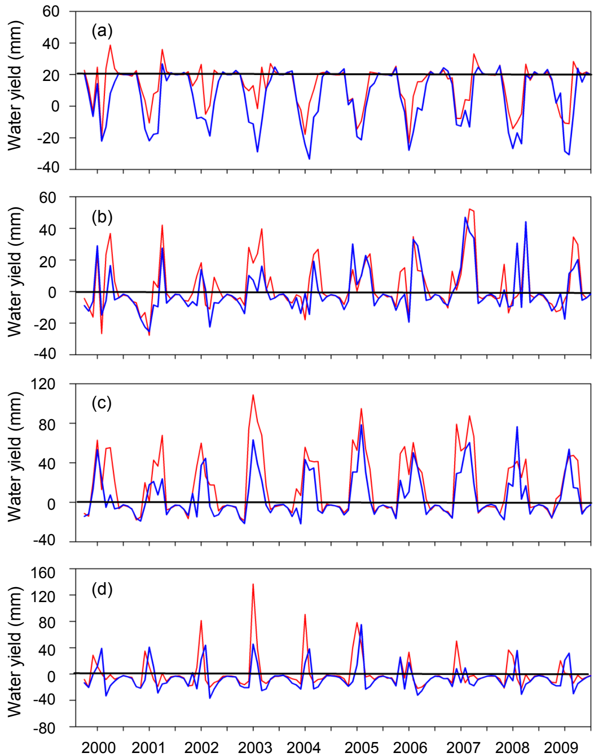


**Figure 10.** Average monthly water yield for 2000–2009; red lines apply to the Shiyang and blue lines to the Hei River watershed. Plots **(a)**–**(d)** coincide with the different elevation zones: **(a)** oasis plains and foothills (Zone 1), and **(b)** low-mountain (Zone 2), **(c)** mid-mountain (Zone 3), and **(d)** high-mountain portions of the watersheds (Zone 4). Note differences in the scale of the *y* axis.